Composites: Part A 104 (2018) 139–150

Contents lists available at ScienceDirect

Composites: Part A

journal homepage: www.elsevier.com/locate/compositesa

Effect of yarn cross-sectional shape on resin flow through inter-yarn gaps in textile reinforcements

A. Endruweit [a,*], X. Zeng [b], M. Matveev [a], A.C. Long [a]

[a] Composites Research Group, Faculty of Engineering University of Nottingham, University Park, Nottingham NG7 2RD, UK
[b] Centre for Future Materials, University of Southern Queensland, West Street, Toowoomba, Queensland 4350, Australia

ARTICLE INFO

Article history:
Received 2 May 2017
Received in revised form 15 October 2017
Accepted 21 October 2017
Available online 28 October 2017

Keywords:
A. Fabrics/textiles
B. Permeability
C. Numerical analysis
E. Resin flow

ABSTRACT

Axial flow through gaps between aligned straight yarns with realistic cross-sectional shapes, described by power-ellipses, was analysed numerically. At a given fibre volume fraction, equivalent gap permeabilities have a maximum at minimum size of elongated tapering parts of the gap cross-section and a ratio of gap width to height near 1. When the yarn spacing is given in addition to the fibre volume fraction, calculated maximum and minimum values for the equivalent permeability of inter-yarn gaps, which occur at near-rectangular and lenticular cross-sections, differ by factors of up to 3.3. Novel approximations for the shape factor and the hydraulic diameter in Poiseuille flow were derived as a function of the fibre volume fraction, the yarn cross-sectional aspect ratio and the geometrical parameter describing the shape of the power-elliptical yarn cross-section. This allows the equivalent gap permeability to be predicted with good accuracy for any fibre volume fraction and yarn cross-section.

1. Introduction

In the manufacture of polymer composite components employing Liquid Composite Moulding (LCM) processes, dry fibrous reinforcements are impregnated with liquid resin systems. To assess the risk of dry spot formation and predict cycle times, the impregnation process is frequently modelled as flow of a viscous liquid through a porous medium, i.e. a network of interconnected hydraulic ducts. Introduction of a macroscopic permeability, as in Darcy's law [1], implies homogenisation of the properties of individual ducts to describe how easily a liquid can flow through the medium. Since the fibre volume fraction, which significantly affects the mechanical properties of finished composite components, is a parameter commonly used for material specification, it is useful to describe the dependence of the permeability of fibrous reinforcements on the fibre volume fraction. The Kozeny-Carman equation [2], which was originally derived for the permeability of porous media consisting of spherical particles, is sometimes used successfully for description of this dependence, albeit with adapted geometrical constants [3]. The frequently cited equations derived by Gebart [4] describe the permeability as a function of the fibre volume fraction for parallel and transverse flow in media with uniform periodic arrangement (square or hexagonal) of aligned fibres. While the spacing of the fibres may vary as a function of the fibre volume fraction, the circular cross-sectional shape of the fibres and the basic fibre arrangement is constant. Hence, Gebart's model does not apply to flow in dual-scale reinforcements made from filaments bundled in deformable yarns, where the yarn shape and reinforcement architecture may change as the fibre volume fraction is varied.

The impregnation of dual-scale reinforcements (fabrics) is determined mainly by resin flow through inter-yarn gaps, since their dimensions are typically large compared to those of intra-yarn gaps [5]. Hence, the permeability of fabric structures can be estimated from analysis of flow through gaps in the fabric architectures. While, strictly speaking, a permeability value is only defined for a porous medium, not for an individual hydraulic duct, it may be convenient to characterise the ratio of average flow velocity and pressure drop in duct flow by an "equivalent permeability". Common examples for flow though individual hydraulic ducts with different cross-sections are discussed in monographs on duct flow [6,7] and textbooks on fluid mechanics [8]. Ni et al. [9] list examples for the equivalent permeability of channels with geometries considered relevant in composites processing. Lundström et al. [10] discuss the permeability of non-crimp fabrics (NCF) and derive an analytical expression for the equivalent permeability of inter-yarn ducts with different cross-sections, including elliptical and parabolic.

* Corresponding author.
E-mail address: andreas.endruweit@nottingham.ac.uk (A. Endruweit).

https://doi.org/10.1016/j.compositesa.2017.10.020
1359-835X/

In a previous study on the permeability of braids [11], the equivalent permeability of inter-yarn gaps was approximated by the permeability of rectangular ducts. To account for the actual duct shape, the permeability was corrected by applying a geometrical factor. It was pointed out that this correction factor is not constant but depends on the effect of yarn deformation, which is caused by through-thickness reinforcement compaction and reinforcement shear. In a recent study [12], a model was presented for the permeability of fabrics consisting of two layers of aligned yarn (as in NCF), subject to deterministic and stochastic non-uniformity. The model was limited by the simplifying assumption that yarns have elliptical cross-sections.

This study systematically assesses the sensitivity of resin flow through inter-yarn gaps in fibrous reinforcements to yarn cross-sectional shapes. To allow this fundamental effect to be identified clearly, the simple example of a single layer of aligned straight yarns was analysed, although, in reality, reinforcements tend to be geometrically more complex. Numerical flow simulation is employed to characterise flow through inter-yarn gaps at different yarn cross-sectional shapes, varying between rectangular and lenticular, and fibre volume fractions. A novel analytical approximation is derived, which allows the equivalent permeability of layers of aligned yarns to be predicted with good accuracy for any fibre volume fraction and yarn shape.

2. Theory

2.1. Reinforcement permeability

For layers of aligned yarns, the permeability parallel to the yarn axes depends on the axial yarn permeability and the equivalent permeability of inter-yarn gaps. It can be approximated by applying a rule of mixtures according to the fraction of the layer cross-sectional area occupied by the gaps, Φ. On the other hand, the in-plane layer permeability perpendicular to the yarn axes is dominated by the transverse yarn permeability. For aligned yarns with minimum inter-yarn gap width (i.e. adjacent yarns are in contact) and no (transverse) fixation, the axial in-plane layer permeability was observed experimentally to be at least one order of magnitude greater than the in-plane permeability perpendicular to the yarn axes [13]. With increasing gap width, the ratio of in-plane layer permeabilities parallel and perpendicular to the yarn axes can be expected to increase. Since the permeability of reinforcement structures comprising several layers of aligned yarns (all at the same orientation or at different orientations) is dominated by axial flow along channels formed between the yarns in each layer, this study focuses on the axial layer permeability.

In the following, the permeability will be discussed for a periodic layer of aligned yarns, where the geometry is characterised by the yarn spacing, s, the yarn thickness, h, and the width, $2R$, of the yarns. The layer can be represented by the repetitive unit cell shown in Fig. 1, where an empty gap is bounded by yarns (left and right) and flat impermeable walls (top and bottom). This may represent a single layer confined between tool surfaces or a layer in a multi-layer structure where no fluid exchange occurs between layers.

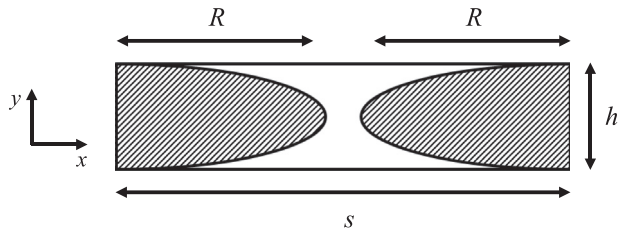

Fig. 1. Abstracted unit cell cross-section with yarns (shaded) and duct (blank); $2R$ is the yarn width, h the yarn thickness, and s the yarn spacing; example: elliptical yarn cross-section.

Applying a rule of mixtures, the axial layer permeability, K_l, can be approximated as

$$K_l = \Phi K_g + (1 - \Phi) K_y, \tag{1}$$

where K_g is the equivalent axial gap permeability, and K_y the axial yarn permeability. For a unit cell with width (yarn spacing), s, and height (yarn thickness), h, the total cross-sectional area is

$$A_{UC} = sh, \tag{2}$$

and the perimeter is

$$P_{UC} = 2s + 2h. \tag{3}$$

If the yarn cross-sectional area is A_y, the fraction of the total cross-sectional layer area occupied by the gap is

$$\Phi = 1 - \frac{A_y}{A_{UC}} \tag{4}$$

The contribution of the axial yarn permeability to the layer permeability is generally small compared to the contribution of the equivalent gap permeability [14] and will be neglected here, i.e.

$$K_l \approx \Phi K_g. \tag{5}$$

2.2. Yarn geometry model

The cross-sectional shape of a multifilament yarn in a fabric structure is determined by effects of through-thickness and lateral compression [15]. Yarn cross-sections may be approximated by generalised power-ellipses [16], which are described by points (x, y) satisfying the equation

$$\left(\frac{x}{R}\right)^2 + \left(\frac{2y}{h}\right)^{2/n} = 1. \tag{6}$$

Here, the parameter in the exponent, n, describes the shape of the power-ellipse. As in Fig. 1, $2R$ is the yarn width, and h is the yarn height. The characteristics of power-ellipses are shown in Fig. 2 for different values of n, resulting in rounded rectangular, elliptical and lenticular shapes.

2.3. Applicability

A unit cell as described above is representative for the gap geometry in preforms from aligned yarns or tapes produced by Automated Fibre Placement (AFP). Since polymeric binder, which may block inter-filament gaps, is typically applied to provide stability to the yarns or tapes, the assumption of negligible permeability of the yarns appears particularly appropriate for this type of preform. Experimental observations documented by Belhaj et al. [17] confirm that the preform permeability is determined by inter-yarn gaps.

The unit cell in Fig. 1 is also similar to that of yarn layers in NCFs, where Eq. (6) was found to be generally a reasonable approximation of yarn cross-sectional shapes [18]. Asymmetry and local random variations [19,20] of yarn cross-sections in fabrics will not be discussed here. In reality, stitching threads are frequently used to provide yarn fixation, which reduce the fabric permeability by locally affecting the inter-yarn gap geometry. This was analysed numerically by Hu et al. [21] and Nordlund and Lundström [22]. In other NCFs, grids ("scrims"), adhesively bonded onto the aligned yarns, are used for yarn fixation. Their effect on the permeability through localised layer compaction was studied experimentally

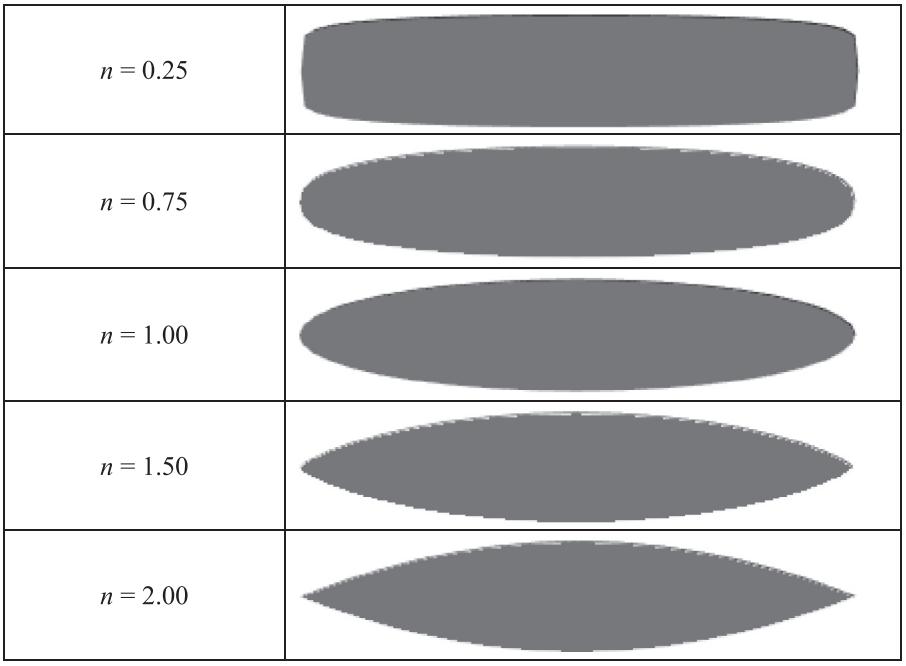

Fig. 2. Examples for generalised power ellipses at given cross-sectional aspect ratio, $2R/h = 5$, for different values of n.

[13]. For both yarn fixation strategies, the localised effect on the permeability can be significant.

Three-dimensional woven reinforcements typically comprise layers of aligned yarns at alternating orientation with additional through-thickness yarns. The example in Fig. 3 shows the network of ducts formed in this type of reinforcement. Each layer can be represented by unit cells as in Fig. 1, while the effect of the through-thickness yarns can be modelled as a local disturbance of the geometry [23].

For other fabrics (e.g. 2D woven or braided), permeability estimation based on a unit cell as in Fig. 1 is less appropriate because of the effect of crimp, although configurations of the type analysed here may be found locally. Generation of detailed geometrical models of multi-layer reinforcements from woven fabrics and lay-up permeability prediction based on these models is addressed elsewhere [24]. However, any model of this kind can only apply to one specific reinforcement, while the purpose of the present study is systematic analysis of the sensitivity of resin flow through inter-yarn gaps to changes in yarn cross-sectional shape. Here, it is necessary to use a simple geometry, although it does not necessarily represent a specific reinforcement at the highest possible accuracy. If more complexity is added, various effects will be superimposed which may obscure the influence of the yarn shape.

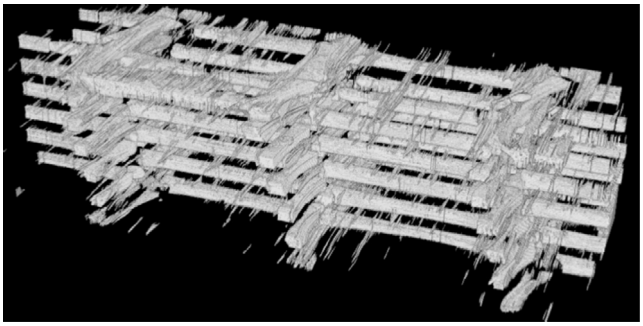

Fig. 3. Network of inter-yarn gaps in 3D orthogonal weave carbon fibre reinforcement, from micro-Computed Tomography data of composite.

2.4. Duct flow analysis

For fully developed laminar flow of an incompressible fluid through a duct with constant cross-section, the Navier-Stokes equations describing the fluid motion reduce to the Poisson equation,

$$\frac{\partial^2 u}{\partial x^2} + \frac{\partial^2 u}{\partial y^2} = \frac{1}{\eta}\frac{\Delta p}{L}. \tag{7}$$

Here, $u(x, y)$ is the local axial flow velocity, assuming that the duct is aligned with the z-direction, η the fluid viscosity, L the length of the duct, and Δp the pressure drop along L. With $u = 0$ on the duct boundary, this equation can be solved numerically to determine $u(x, y)$, from which the average flow axial velocity, v, can be calculated. Applying Darcy's law (for the case of uni-directional flow in a porous medium) to axial flow in a single duct, the equivalent axial duct permeability,

$$K_g = \frac{v\eta L}{\Delta p}, \tag{8}$$

can be determined. To describe the pressure loss in viscous flow along a hydraulic duct (Darcy-Weisbach equation), the equivalent permeability can be identified as

$$K_g = \frac{2D_h^2}{c}. \tag{9}$$

Here, D_h is the hydraulic diameter of the gap. It is defined as

$$D_h = \frac{4A_g}{P_g}, \tag{10}$$

where A_g is the gap cross-sectional area and P_g the perimeter of the gap cross-section. D_h is a measure for the relative effect of the perimeter (the axial flow velocity is zero on the gap boundary) on flux along the duct. The quantity c in Eq. (9) is a shape factor, corresponding to four times the Poiseuille number. It can be expressed as the product of the Darcy friction factor,

$$f_D = \frac{2D_h}{\rho_f v^2}\frac{\Delta p}{L}, \tag{11}$$

which indicates the ratio between the local shear stress and the local kinetic energy density, and the Reynolds number,

$$Re = \frac{\rho_f v D_h}{\eta}, \tag{12}$$

i.e. the ratio of inertial forces and viscous forces, for the respective flow problem. In Eqs. (11) and (12), ρ_f is the density of the fluid. The value of c is a measure for the effect of viscous friction on flux. Hence, it is related to the length of boundaries between fluid layers moving at different velocity in laminar flow, which in turn depends on the flow velocity distribution across the duct cross-section.

While flow through ducts with a wide variety of cross-sections is discussed in the literature [7], only a special case of the geometry described above was analysed by Gunn and Darling [25]. Here, the ultimate aim is to derive generalised analytical approximations for c and D_h as a function of geometrical duct parameters, which would allow equivalent gap permeabilities to be predicted for any power-elliptical yarn cross-sectional shape.

3. Numerical flow simulation

3.1. Method

Here, modelling yarn geometries as described above in TexGen [26] was combined with numerical analysis in Ansys® CFX®, where a finite volume method is implemented, to solve the duct flow problem described above. Using pre-defined functions for the yarn cross-sections, three-dimensional geometrical models of inter-yarn gaps (length along yarn axis L = 0.05 mm) were generated and meshed with tetrahedral cells. Translational periodicity was applied along the yarn direction to represent continuous parallel yarns with constant cross-section. Hence, the solution is independent of the model length. No-slip wall boundary conditions, i.e. u = 0, were applied on the entire gap perimeter. At the top and bottom boundaries of the duct, this is consistent with the presence of impermeable walls. Since inter-yarn gaps are typically one order of magnitude larger than pore spaces in the yarns [5,27], and the flow velocity in the yarns is small compared to the flow velocity in the inter-yarn gap, no-slip boundary conditions were also applied on the yarn surfaces, i.e. the left and right boundaries of the gap. Use of a slip boundary condition [28] would be essential if the dimensions of inter-yarn gaps were comparable to the dimensions of intra-yarn pores, and intra-yarn flow contributed significantly to the permeability of the yarn layer (Nedanov and Advani [14] report that the effect of intra-yarn flow is small, even at relatively small inter-yarn porosity down to 0.13). The assumption of steady state (saturated) flow implies that transient capillary effects, which in reality may affect the applied flow-driving pressure gradient during reinforcement impregnation (as documented e.g. by Pillai [29]), were not considered in the simulations.

For a given axial pressure gradient, $\Delta p/L$, and fluid viscosity, η, the average axial flow velocity, v, in the inter-yarn duct was calculated from the flow velocities, u_i, and the areas, A_i, of cells representing the cross-section, A_g, according to

$$v = \frac{\sum_i u_i A_i}{A_g}. \tag{13}$$

The equivalent axial channel permeability was determined from v according to Eq. (8). A mesh sensitivity study, where two unit cell geometries were analysed (one with s = 0.65 mm and h = 0.84 mm, the other with s = 1.96 and h = 0.28 mm; both at n = 1.00 and Φ = 0.40), indicated that the solution converged if the average edge length of cells in the numerical simulations was 0.01 mm or less.

3.2. Validation

Before new results were generated for geometries described above, the numerical method employed here for flow simulation and permeability calculation was validated for the example of a duct with rectangular cross-section, for which K_g can be expressed analytically. The equivalent permeability of a rectangular duct is given by Eq. (9), where D_h is easy to calculate. The dependence of the shape factor on the aspect ratio, ρ, can be approximated [12] by the relation

$$c = 56.4\rho^{0.17}, \tag{14}$$

which is based on data tabulated by White [8]. In Eq. (14), the duct cross-sectional aspect ratio is defined as

$$\rho = \begin{cases} h/(s-2R), & \text{if } (s-2R) \leqslant h \\ (s-2R)/h, & \text{if } (s-2R) > h \end{cases} \tag{15}$$

Alternatively, the equivalent permeability can be expressed as

$$K_g = \frac{h^2}{12}\left(1 - \frac{192h}{\pi^5(s-2R)}\sum_{i=1,3,5\ldots}^{\infty}\frac{\tanh(i\pi(s-2R)/2h)}{i^5}\right), \tag{16}$$

which is the analytical solution of the Navier-Stokes equation for flow through a rectangular duct with no-slip boundary conditions on all walls [30].

The values for K_g listed in Table 1 indicate that agreement between results from the numerical simulations and from Eq. (16), where five terms were considered in the approximation, is very good (less than 1% difference). The slight difference (less than 3%) between simulation results and results from Eq. (9) can be explained by the fact that the approximation for the shape factor in Eq. (14) may show some local deviation from the actual value of c. Based on comparison with the theoretical approximations in Eq. (9) and in Eq. (16), it can be concluded that the numerical simulation results are plausible, and that the proposed method is suitable for quantitatively analysing duct flow.

4. Results and discussion

4.1. Characteristics of equivalent duct permeability

Unit cell models with different yarn cross-sectional shapes were analysed here. Values of n were varied between 0.25 and 2.00, which corresponds to rounded rectangular and lenticular cross-sections, respectively (Fig. 2). While the yarn cross-sectional area, A_y, was kept constant at 0.33 mm^2, values for the gap volume fraction, Φ, were set (between 0.07 and 0.50) through appropriate combination of the geometrical parameters. A total of 239 models were analysed. To facilitate discretisation of the tapering elongated parts of the inter-yarn gap, a minimum width of 1.5×10^{-3} mm was enforced. This does not have a significant effect on A_g or P_g, and the induced error in calculated permeabilities is small.

Examples for equivalent permeability values derived from numerical simulations at Φ = 0.50 and Φ = 0.30 are plotted in Fig. 4 as a function of s at different values of n. To realise the selected combinations of n and Φ, the yarn width, $2R$, was varied between 0.50 mm and 3.50 mm, the yarn height, h, between 0.10 mm and 0.99 mm, and the yarn spacing, s, between 0.51 mm and 6.33 mm. The yarn spacing was selected as independent variable since its values can in reality be obtained relatively easily through measurement, and it can typically be set in manufacture of

Table 1
Comparison of equivalent permeability, K_g, for a rectangular duct with given width and height, derived from numerical simulation and analytical approximations.

Width/mm	Height/mm	Aspect ratio	$K_g/10^{-10}$ m^2		
			Simulation	Eq. (9)	Eq. (16)
0.16	0.71	4.39	18.80	19.22	18.77

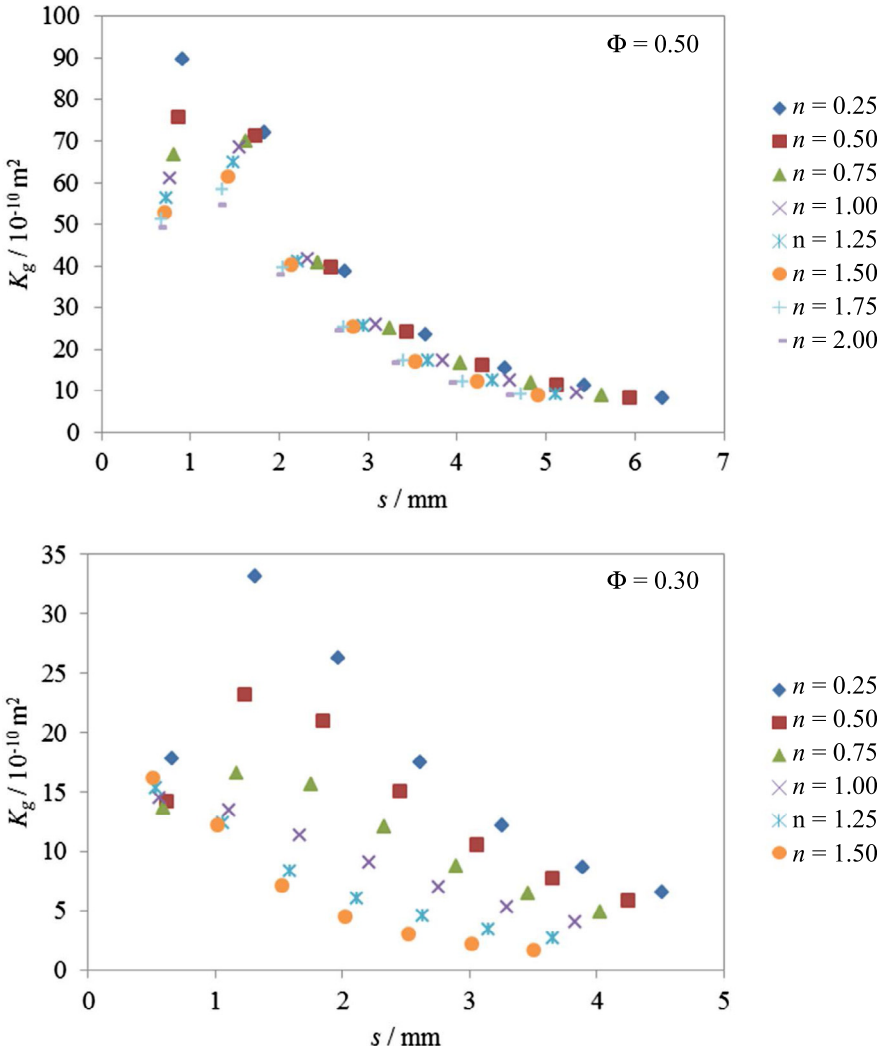

Fig. 4. Equivalent duct permeability, K_g, as a function of the yarn spacing, s, at different gap volume fractions, Φ, and different geometrical parameters, n. (For interpretation of the references to color in this figure legend, the reader is referred to the web version of this article.)

reinforcements (e.g. in textile processes). In the diagram for Φ = 0.30, the range of n is narrower than for Φ = 0.50 since adjacent yarns are in contact with each other where the condition $2R = s$ is met. Hence, Φ = 0.30 cannot be obtained for yarns with lenticular cross-section (n = 1.75 and n = 2.00). Minimum obtainable values of the gap volume fraction, Φ_{min} (at $2R = s$), are listed in Table 2.

The data in Fig. 4 indicate that, as expected, K_g decreases with decreasing Φ at given s and n, since the total gap cross-sectional area decreases. There is a trend for the gap permeability to decrease with increasing n, implying that K_g is higher if the yarn cross-sections are rectangular than if they are lenticular. The equivalent permeability as a function of the yarn spacing shows a maximum, the position of which depends on Φ and n. In Figs. 5 and 6, this is illustrated for two examples, where the equivalent permeability is related to gap geometries and resulting flow velocity distributions. The gap geometry is characterised by the yarn cross-sectional aspect ratio, $2R/h$, the yarn spacing, s, and the aspect ratio of the largest rectangle that can be inscribed in the gap, ρ, defined according to Eq. (15).

Table 2
Minimum obtainable gap volume fraction, Φ_{min}, at different values of n (at $2R = s$).

n	Φ_{min}
0.25	0.07
0.50	0.13
0.75	0.17
1.00	0.21
1.25	0.25
1.50	0.28
1.75	0.31
2.00	0.33

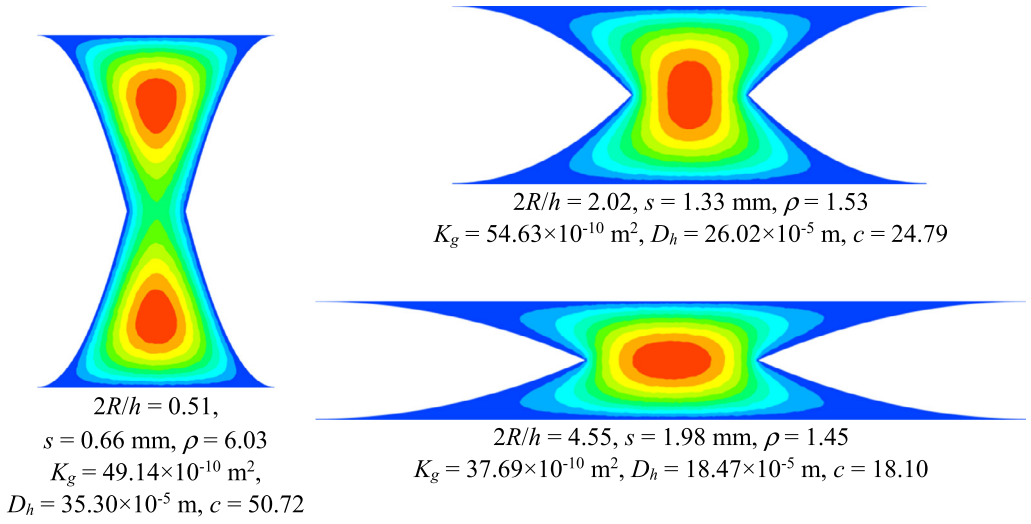

Fig. 5. Results of numerical simulations at $\Phi = 0.50$, $n = 2.00$; different yarn cross-sectional aspect ratio, $2R/h$, yarn spacing, s, and gap cross-sectional aspect ratio, ρ, as defined in Eq. (15); contours indicate different axial flow velocity distributions in inter-yarn gaps (qualitatively); equivalent permeabilities, K_g, hydraulic diameters, D_h, and shape factors, c, are also given. (For interpretation of the references to color in this figure legend, the reader is referred to the web version of this article.)

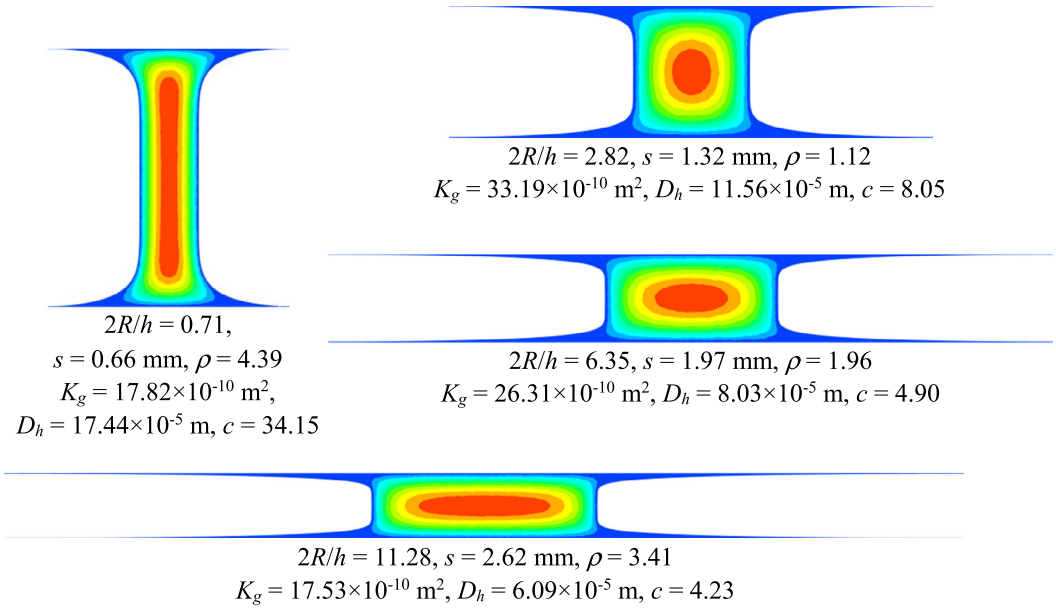

Fig. 6. Results of numerical simulations at $\Phi = 0.30$, $n = 0.25$; different yarn cross-sectional aspect ratio, $2R/h$, yarn spacing, s, and gap cross-sectional aspect ratio, ρ, as defined in Eq. (15); contours indicate different axial flow velocity distributions in inter-yarn gaps (qualitatively); equivalent permeabilities, K_g, hydraulic diameters, D_h, and shape factors, c, are also given. (For interpretation of the references to color in this figure legend, the reader is referred to the web version of this article.)

For $n = 2.00$, i.e. lenticular yarn cross-sections, Fig. 5 shows one maximum in the flow velocity distribution if s is greater than approximately 1.32 mm. On the other hand, there are two maxima in the flow velocity distribution for $s < 1.32$ mm. This qualitative change in axial flow velocity distribution is consistent with the data plotted in Fig. 4, where K_g (at $\Phi = 0.50$ and $n = 2.00$) has a maximum at $s = 1.32$ mm and decreases towards larger and smaller values of s. For yarns with almost rectangular cross-sections, i.e. $n = 0.25$, Fig. 6 shows that the gap between yarns is approximately square ($\rho = 1.12$) for $s = 1.32$ mm. This coincides with the maximum in calculated equivalent permeability values (Fig. 4, at $\Phi = 0.30$ and $n = 0.25$). While a transition in the flow velocity distribution from one maximum to two maxima can be observed for all combinations of Φ and n when s is reduced, here it occurs at a value of s smaller than 0.66 mm. Hence, the examples in Fig. 6 do not include a case with two maxima. Figs. 5 and 6 are consistent with results presented in a recent study [12] for the case with $n = 1.00$, where Φ was varied through variation of $2R/h$ at constant s, and similar flow velocity distributions as shown here (with either one or to two maxima) were found.

A quantitative comparison of flow through an almost rectangular duct (Fig. 6, $\Phi = 0.30$, $n = 0.25$, $s = 0.66$ mm) and a rectangular duct with identical values of $s - 2R$ and h (Table 1) is presented in Table 3. While the cross-sectional area is larger for the duct with $n = 0.25$ than for the rectangular duct, the average flow velocity in Eq. (8) is smaller (at identical values for η, Δp and L). This indicates that the tapering elongated parts of the duct cross-section (for $n = 0.25$) contribute to the cross-sectional area, but not significantly to flux. As a result, the equivalent permeability is smaller for the duct with $n = 0.25$ than for the rectangular duct. This illustrates that

Table 3
Cross-sectional area, A_g, average flow velocity, v, equivalent permeability, K_g, for ducts with s-$2R$ = 0.16 mm and h = 0.71 mm, but different cross-sectional geometry.

Geometry	A_g/mm^2	v/mm/s	K_g/10^{-10} m^2
n = 0.25	0.14	1.92	17.82
Rectangular	0.12	2.02	18.80

increasing duct cross-sectional area does not necessarily translate into increasing equivalent permeability.

For rectangular ducts at given total duct cross-sectional area, K_g is determined by the aspect ratio, ρ, and is independent of the orientation of the long and short duct cross-sectional axes. On the other hand, Fig. 6 shows that this is not the case for ducts with n = 0.25, where values for K_g are almost identical at s = 0.66 mm and s = 2.62 mm, but the corresponding values of ρ are different.

Table 4 summarises maximum and minimum equivalent permeabilities, K_{gmax} and K_{gmin}, for the data plotted in Fig. 4. If K_{gmax} and K_{gmin} are picked from the entire range of s, i.e. if they correspond to different values of s and n, K_{gmax}/K_{gmin} has values of up to approximately 20 (at Φ = 0.30, where K_{gmax}/K_{gmin} is the highest). If, at given gap volume fraction, K_{gmax} and K_{gmin} are picked at the same value of s (such that they lie on the same vertical line in Fig. 4), the ratio K_{gmax}/K_{gmin} can still have values of up to 3.3 (at Φ = 0.30). In this case, the difference between K_{gmax} and K_{gmin} is caused only by the yarn cross-sectional shape. This is consistent with experimental results from a recent study [31], where specimens of a twill weave fabric were repeatedly sheared to defined angles and then unsheared. After being subjected to sequences of defined shear operations, increases in inter-yarn gap width at constant yarn spacing were observed, which translated into increases in measured fabric permeabilities by factors of up to 2 compared to the virgin material (at identical fibre volume fraction). The experimental observations for the twill weave fabric confirm that the shape of inter-yarn gaps has a significant effect on the in-plane permeability of a reinforcement, even if the actual yarn arrangement is geometrically more complex than in the straight aligned layers analysed here. On the other hand, the difference in factors between maximum and minimum permeability (factors 3.3 for the equivalent gap permeability in the simulations and approximately 2 for the fabric permeability in the experiments) reflects the influence of different fibre volume fractions (Φ = 0.30 in the simulations; in the experiments, the global porosity was 0.44) and of geometrical features such as crimp, which is not considered in the simulations. It is thought that the effect of variation in gap shape between specimens contributes (among other factors) to the occasionally very significant scatter observed in experimentally acquired permeability data of macro-scale fabric specimens [32]. Fig. 4 also indicates that values of K_g at different n converge for large s, implying that the effect of yarn shape is reduced with increasing width of inter-yarn gaps.

For the special case with n = 1.00, Lundström et al. [10] presented an analytical approximation for the equivalent permeability of ducts as described above. Comparison of the proposed approximation with simulation results, for all 28 examples with n = 1.00 evaluated here, indicates that equivalent permeabilities are predicted with good accuracy for large values of Φ (at Φ = 0.50, the coefficient of correlation, R^2, is 0.998). On the other hand, differences between simulation results and predictions become significant when Φ is reduced (R^2 = 0.533 at Φ = 0.30). This is thought to be related to changes in flow velocity distributions at small gap widths, which are not described by the predictions.

4.2. Analytical characterisation of duct flow

To characterise duct flow in terms of hydraulic diameter and shape factor, D_h is calculated by substituting the geometrical parameters of the flow channel, P_g and A_g, in Eq. (10), and c is determined according to Eq. (9), where K_g is obtained from simulations. A general relation between the duct cross-sectional area, A_g, and the yarn cross-sectional area, A_y, as illustrated in Fig. 1, is

$$A_g = A_{UC} - A_y. \tag{17}$$

Similarly, the relation between the duct perimeter, P_g, and the yarn perimeter, P_y, is

$$P_g = 2s + P_y. \tag{18}$$

Here, A_g and P_g are calculated numerically, which is facilitated by discretisation of the geometry (Fig. 1) for flow simulation to determine K_g. Meshing of the geometry results in the perimeter of the power ellipse to coincide with a closed loop formed by cell edges. Approximating the perimeter by the total length of the corresponding cell edges allows P_g to be determined according to Eq. (18). The value of A_g can be approximated directly by summarising the areas of cells representing the gap cross-section.

Since, at given Φ, combinations of values for $2R$, h, s and n are unique, duct cross-sectional shapes are fully characterised by three parameters: The gap volume fraction, Φ, the aspect ratio of yarn width to yarn height, $2R/h$, and the geometrical parameter, n. Values for c are plotted in Fig. 7 as a function of $2R/h$ at different values of n for the example of Φ = 0.30, and in Fig. 8 as a function of Φ at different values of $2R/h$ for the example of n = 0.25. The hydraulic diameter, D_h, is plotted in Fig. 9 as a function of $2R/h$ at different values of n for the example of Φ = 0.30 (corresponding to Fig. 7).

Fig. 7 indicates that c decreases with increasing value of $2R/h$ and decreasing n. Similarly, Fig. 9 indicates that D_h decreases with increasing $2R/h$, while the effect of n on D_h is very small. The steep gradients for small $2R/h$ (c drops from 34.2 at $2R/h$ = 0.71 to 8.1 at $2R/h$ = 2.82 for the example of n = 0.25) reflect the quick increase in perimeter length at constant cross-sectional area and its effect on the flow velocity distribution with increasing $2R/h$. On the other hand, c is approximately constant for $2R/h$ > 10. This indicates that, in this range, flow characteristics are identical for ducts with similar cross-sectional shape but different dimensions, as discussed by Mortensen et al. [33]. Values of D_h decrease only by small amounts for $2R/h$ > 10. In reality, cross-sectional aspect ratios of yarns in reinforcement fabrics are frequently in this range. Figs. 5 and 6 relate the significant drop in values for c and D_h to changing duct cross-sections and flow velocity distributions as $2R/h$ is increased.

Table 4
Minimum and maximum calculated permeability values, K_{gmin} and K_{gmax}, and ratio, K_{gmax}/K_{gmin}, at different gap volume fractions, Φ; K_{gmin} and K_{gmax} are picked either from the entire range of s, or at the same value of s; for the latter case, K_{gmin} and K_{gmax} are listed for the value of s where K_{gmax}/K_{gmin} has a maximum at the respective Φ.

Φ	K_{gmin}/10^{-10} m^2	K_{gmax}/10^{-10} m^2	Based on	K_{gmax}/K_{gmin}
0.50	8.00	89.26	Entire range of s	11.15
	54.63	89.26	s = 0.93 mm	1.74
0.30	1.67	33.19	Entire range of s	19.85
	8.92	33.19	s = 1.32 mm	3.27

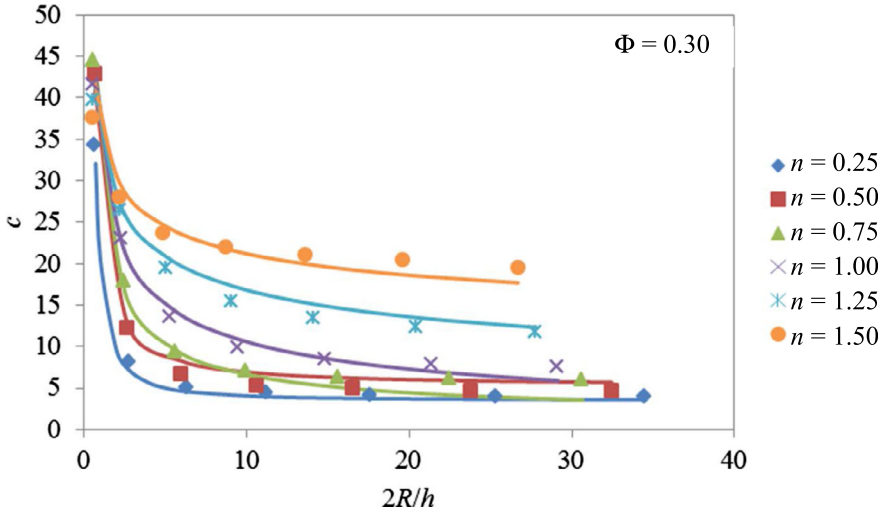

Fig. 7. Shape factor, c, as a function of the yarn cross-sectional aspect ratio, $2R/h$, at different geometrical parameters, n; gap volume fraction $\Phi = 0.30$; markers indicate results from numerical analysis, lines represent analytical approximation described in Section 4.2. (For interpretation of the references to color in this figure legend, the reader is referred to the web version of this article.)

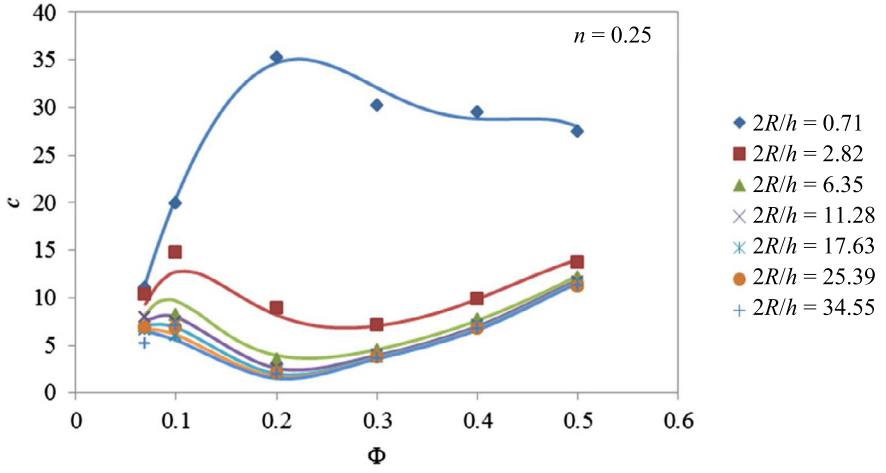

Fig. 8. Shape factor, c, as a function of the gap volume fraction, Φ, at different yarn cross-sectional aspect ratios, $2R/h$; geometrical parameter $n = 0.25$; markers indicate results from numerical analysis, lines represent analytical approximation described in Section 4.2. (For interpretation of the references to color in this figure legend, the reader is referred to the web version of this article.)

In Fig. 8, the yarn shape stays the same for each value of $2R/h$, while the yarn spacing is changed to vary Φ. Starting at small values of Φ, c increases until a maximum is reached, which is related to changes in flow patterns at the transition from two maxima in the flow velocity distribution to one maximum. The maximum in c is shifted towards higher values of Φ with decreasing value of $2R/h$. When Φ is increased further, c goes through a local minimum. Since the minimum coincides with approximately square duct cross-section (as in Fig. 6, for $s = 1.32$ mm), it is shifted to higher values of Φ as the ratio $2R/h$ is decreased. D_h decreases monotonously with decreasing Φ, since this implies a reduction in duct cross-sectional area.

The special case with $n = 1.00$, $2R/h = 1$, and $s = 2R$, which corresponds to a gap between yarns with circular cross-section at $\Phi_{min} = 0.21$, was also analysed by Gunn and Darling [25] employing a finite difference method. They found a Poiseuille number of 6.5 (i.e. $c = 26$), which is in good agreement with simulation results obtained here (where $c = 25.5$).

To predict duct flow characteristics, Bahrami et al. [34] approximated c analytically for a selection of convex duct geometries, based on the duct cross-sectional area, perimeter and polar moment of inertia (exploiting the analogy to torsion of a bar, where stress distributions are also described by the Poisson equation, Eq. (7)). However, analysis of several examples for flow through a gap between yarns with power-elliptical cross-section suggested that the proposed method fails to produce values of c which are in satisfactory agreement with values derived from simulations. It is thought that this is related to the simplification of results obtained in torsion theory for prismatic bars, which is implied in the analytical approximation. In particular, the stresses in torsion, expressed in terms of the moment of inertia, are exact only for bars of a circular cross-section and become inaccurate for concave cross-sections. For reference, the derived equations, which may be of use elsewhere, are compiled in Table 5.

In a recent study, where only the special case with $n = 1.00$ was considered, the dependence of the shape factor, c, on the aspect ratio of the yarn cross-section, $2R/h$, was modelled as a power function [12]. Since more data are available here than in the limited study for $n = 1.00$, a generalised approximation for c was found,

$$c = B_1 (2R/h)^{-B_2} + B_3. \tag{19}$$

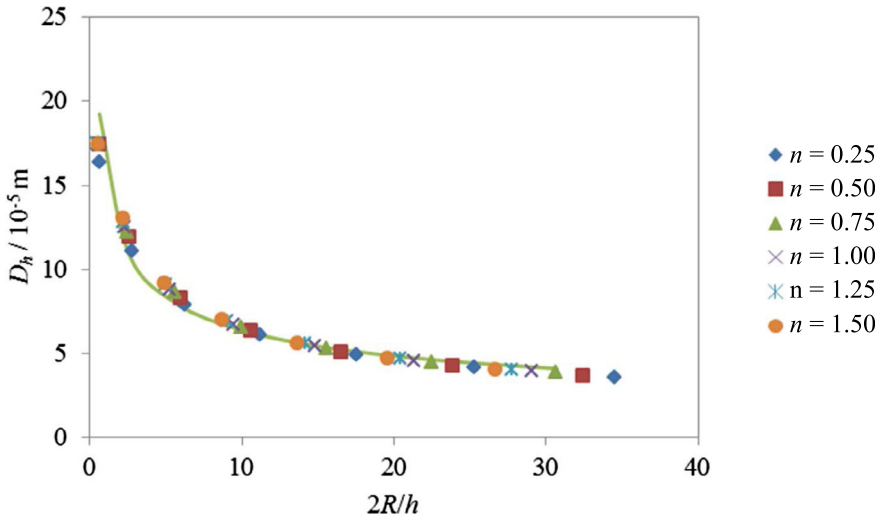

Fig. 9. Hydraulic diameter, D_h, as a function of the yarn cross-sectional aspect ratio, $2R/h$, at different geometrical parameters, n; gap volume fraction $\Phi = 0.30$; markers indicate data from numerical analysis, the line represents the analytical approximation for $n = 0.75$ (as described in Section 4.2). (For interpretation of the references to color in this figure legend, the reader is referred to the web version of this article.)

Table 5
Set of equations to approximate the shape factor, c, as suggested by Bahrami et al. [34] for flow through a gap between yarns with power-elliptical cross-section (characterised by geometrical parameter, n); yarn width, $2R$, yarn height, h, yarn spacing, s.

Geometrical parameter	Analytical expression
Shape factor	$c = 4 \times 128\pi^2 \frac{I_{pg}}{A_g P_g^2}$
Gap cross-sectional area	A_g, see Eq. (17)
Gap perimeter	P_g, see Eq. (18)
Polar moment of inertia of inter-yarn gap	$I_{pg} = I_{yg} + \frac{sh^3}{96} - I_{xy}$
Moment of inertia of gap relative to y-axis	$I_{yg} = \frac{sh^3}{24} - 2\left(\frac{I_{yy}}{2} + \frac{A_y}{2}\left(\left(\frac{s}{2} - \frac{2R^2 h}{(n/2+1)A_y}\right)^2 - \left(\frac{2R^2 h}{(n/2+1)A_y}\right)^2\right)\right)$
Moment of inertia of yarn relative to y-axis	$I_{yy} = \frac{1}{2} nR^3 h \sqrt{\pi} \frac{\Gamma(n/2)}{\Gamma((n+5)/2)}$
Moment of inertia of yarn relative to x-axis	$I_{xy} = \frac{1}{8} nRh^3 \sqrt{\pi} \frac{\Gamma(3n/2)}{\Gamma(3(n+1)/2)}$
Yarn cross-sectional area [35]	$A_y = Rh\sqrt{\pi} \frac{\Gamma((n+2)/2)}{\Gamma((n+3)/2)}$
Yarn perimeter, $n \geq 2$	$P_y = 4\sum_{i=1}^{\infty} \frac{R}{2} \left(\frac{nh}{2R}\right)^{2i} \binom{1/2}{i} \mathrm{B}(i + 1/2, ni - 2i + 1)$
Yarn perimeter, $0 \leq n < 2$	$P_y = 4\sum_{i=1}^{\infty} \sum_{k=1}^{\infty} \frac{R}{2i+2k+1} \left(\frac{nh}{2R}\right)^{2i} \binom{1/2}{i} \binom{k + 2i - ni - 1}{2i - ni - 1}$ Here, Γ and B are the Gamma- and Beta-function, respectively

Here, the dependence of B_i on Φ can be approximated by fourth-order polynomials,

$$B_i = \sum_{j=1}^{5} B_{ij} \Phi^{5-j}. \tag{20}$$

Similarly, the dependence of B_{ij} on n can be approximated by

$$B_{ij} = \sum_{k=1}^{5} B_{ijk} n^{5-k}. \tag{21}$$

The coefficients B_{ijk} (63 different non-zero values), which allow approximations of c to be calculated for any given combination of n, $2R/h$ and Φ, are listed in Table 6. The examples plotted in Figs. 7 and 8 show that the quality of the approximation described by Eqs. (19) to (21) is generally satisfying. The fit to values of c as a function of $2R/h$ (at $\Phi = 0.30$) is characterised by coefficients of correlation (R^2) between 0.994 and 1.000 (for different values of n). Coefficients of correlation for the fit to values of c as a function of Φ (at $n = 0.25$) are between 0.910 and 0.993 (for different values of $2R/h$).

For the dependence of D_h on Φ, the expression

$$D_h = E_1 \Phi^3 + E_2 \Phi \tag{22}$$

was found. Here, the dependence of E_i on $2R/h$ and n can be approximated by

$$E_i = E_{i1} (2R/h)^{E_{i2}}. \tag{23}$$

and

$$E_{ij} = \sum_{k=1}^{4} E_{ijk} n^{4-k}. \tag{24}$$

Values for the 16 coefficients, E_{ijk}, are listed in Table 7. The quality of the fit of Eqs. (22)–(24) with the coefficients E_{ijk} to values of D_h is generally good. For the example in Fig. 9 ($\Phi = 0.30$ and $n = 0.75$), the coefficient of correlation for D_h as a function of $2R/h$ has a value of 0.974.

4.3. Implications for reinforcements at changing fibre volume fraction

If the fibre volume fraction in a reinforcement is increased in through-thickness compaction, the effect on the yarn cross-sectional shape is generally not known. A decrease in h to reduce Φ could result in a change in $2R$, n, or both. The yarn deformation mechanisms may also differ for different reinforcements. The problem is simplified when adjacent yarns are in contact, i.e. R can be assumed to be constant, and n decreases with decreasing h. On the other hand, if the fibre volume fraction is increased by reducing s, e.g. in shear or lateral reinforcement compression, h, R and n can be assumed to be constant as long as $2R < s$. Once adjacent yarns are in contact, R and n decrease with decreasing s.

For illustration, Figs. 10 and 11 show the permeability of a reinforcement layer, K_l, as a function of Φ, which was calculated according to Eq. (5) from additional simulation results for K_g. For both examples (14 simulations each), the yarn cross-sectional area,

Table 6
Values of coefficients, B_{ijk}, for approximation of the shape factor, c, according to Eqs. (19)–(21).

	k				
ij	1	2	3	4	5
11	0	0	0	0	−7118
12	−9061	10,370	21,060	−18,630	12,630
13	13,630	−24,620	−8414	13,880	−7031
14	−6641	15,360	−4511	−1639	1302
15	1048	−2831	1741	−320.7	−17.84
21	0	0	0	0	−333
22	−241.3	588.9	−323	221.1	314.8
23	320.1	−834.1	525.3	−287.1	−62.11
24	−139.8	386.8	−268.4	115.3	−11.39
25	20.12	−58.99	44.3	−14.11	1.43
31	0	0	0	0	1161
32	12,330	−24,650	−1036	11,410	−3841
33	−16,850	38,600	−11,060	−7771	2738
34	7651	−19,730	10,650	−18.79	−490.2
35	−1153	3293	−2427	525.2	−20.34

Table 7
Values of coefficients, E_{ijk}, for approximation of the hydraulic diameter, D_h, according to Eqs. (22)–(24).

	k			
ij	1	2	3	4
11	-14.330×10^{-5} m	54.138×10^{-5} m	-71.849×10^{-5} m	94.514×10^{-5} m
12	−0.004	−0.010	0.079	−0.591
21	3.441×10^{-5} m	-12.828×10^{-5} m	14.418×10^{-5} m	42.258×10^{-5} m
22	−0.009	0.037	−0.026	−0.382

A_y = 0.33 mm^2, was assumed to be constant. At Φ = 0.33, the geometry was characterised by n = 2.00, s = 1.98 mm, 2R = 1.98 mm, and h = 0.25 mm. Fig. 10 illustrates the case of through-thickness compaction, where s is constant. For 2R < s, 2R is increased from 1.34 mm to 1.83 mm to compensate for a reduction in h from 0.37 mm to 0.27 mm, while n = 2.00 is assumed to be constant here. For 2R = s, n is reduced from 2.00 to 0.25 to allow 2R and A_y to stay constant, while h is reduced from 0.25 mm to 0.18 mm (as also proposed by Swery et al. [36]). In Fig. 11, the case of reducing yarn spacing, which may occur when a uni-directional layer is sheared, is illustrated, where h is constant. For 2R < s, 2R is constant at 1.98 mm and n = 2.00, while s is reduced from 3.00 mm to 2.00 mm. When adjacent yarns are in contact, 2R and s are reduced simultaneously from 1.98 mm to 1.42 mm, and n is reduced from 2.00 to 0.25 to allow A_y to stay constant.

Comparison of the two examples indicates that, at identical Φ, K_l has greater values in lateral compression than in through-thickness compaction if Φ < 0.33. On the other hand,

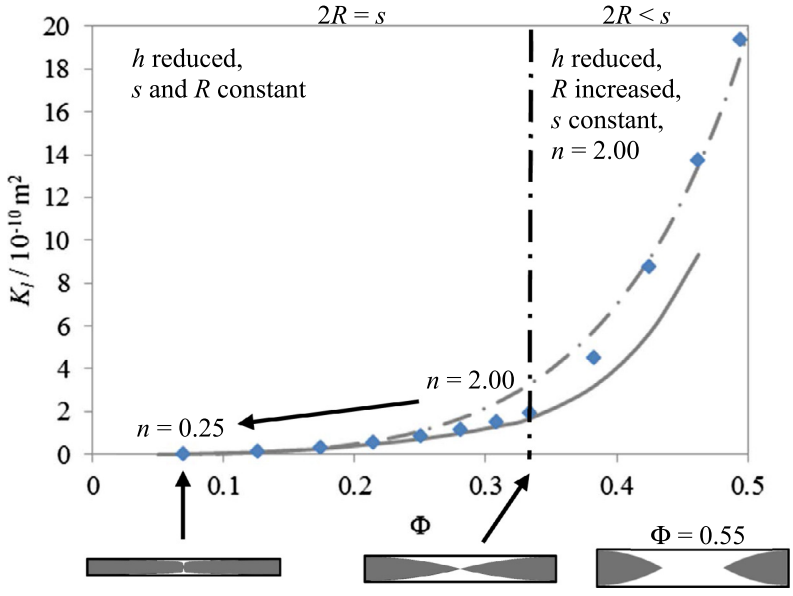

Fig. 10. Permeability of a reinforcement layer, K_l, as a function of porosity, Φ; porosity is reduced in through-thickness compaction, i.e. through reduction of h; markers indicate simulation results (data points for Φ > 0.50 are omitted); continuous line indicates approximation based on c and D_h (Section 4.2); dashed line indicates approximation according to Eq. (25) with $F = 39 \times 10^{-10}$ m^2. (For interpretation of the references to color in this figure legend, the reader is referred to the web version of this article.)

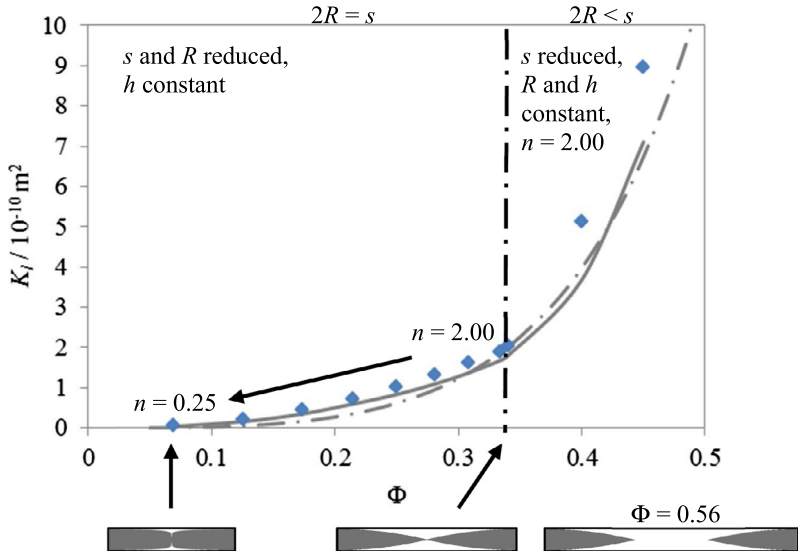

Fig. 11. Permeability of a reinforcement layer, K_l, as a function of porosity, Φ; porosity is reduced through reduction of s; markers indicate simulation results (data points for Φ > 0.50 are omitted); continuous line indicates approximation based on c and D_h (Section 4.2); dashed line indicates approximation according to Eq. (25) with $F = 22 \times 10^{-10}$ m^2. (For interpretation of the references to color in this figure legend, the reader is referred to the web version of this article.)

if Φ > 0.33, K_l is greater in through-thickness compaction. Although the values of K_l are identical at Φ = 0.33, the mechanism for changing Φ has a significant effect on the reinforcement permeability.

In addition, values for K_l were predicted based on the approximations for c and D_h described above. In the range with Φ < 0.50, for which the approximations were derived, the coefficient of correlation between predicted values and simulation results is 0.997 for the case of through-thickness compaction (Fig. 10). For the case of lateral compaction (Fig. 11), it is 0.995. The predictions show generally good quantitative agreement with simulation results, in particular for small Φ.

The figures also show curves indicating approximations for $K_l(\Phi)$ based on Gebart's equation for axial flow in aligned fibrous media,

$$K_l = F\frac{\Phi^3}{(1-\Phi)^2}, \tag{25}$$

which was devised for fibres with circular cross-section and regular periodic arrangement (the same dependence on Φ was formulated by Cozeny-Karman [2]). The factor F depends on the fibre radius and the shape factor, c, as defined above. In Figs. 10 and 11, F was replaced by (constant) fitting factors. Although Gebart's approximation cannot quantitatively predict appropriate values of F for flow through inter-yarn gaps, the fitted trend curve for $K_l(\Phi)$ according to Eq. (25) shows good agreement (R^2 = 0.996) with values derived from simulations if Φ is changed in though-thickness compression (Fig. 10). However, if Φ is changed in lateral compression (Fig. 11), the fitting factor, F, is significantly different, and the dependence of K_l on Φ is not approximated with the same accuracy (R^2 = 0.965). This indicates that, to obtain reliable results, describing the permeability of a reinforcement as a function of the fibre volume fraction only is not sufficient, and an approximation as derived in Section 4.2 is required.

The extensive analysis presented here lends itself to further enhance the predictive capabilities of a recent model for the permeability of fabrics with deterministic and stochastic non-uniformity [12], where the fibre volume fraction and the shape of inter-yarn gaps vary locally, through elimination of the limiting assumption that yarns have elliptical cross-sections.

5. Conclusion

For examples of single layers of aligned straight yarns, axial duct flow through gaps between adjacent yarns was analysed employing numerical simulations. Yarn cross-sectional shapes, which were different for each example, were approximated by power ellipses. The simulations indicate that, at given fibre volume fraction, equivalent duct permeabilities have a maximum, when the size of elongated tapering parts of the duct cross-section has a minimum, and the ratio of duct width to duct height is near 1. As a rule of thumb, higher equivalent permeabilities can be obtained for ducts bounded by yarns with near-rectangular cross-section than by yarns with lenticular cross-section. This implies also that increasing the duct cross-sectional area by changing the duct shape does not necessarily translate into increasing equivalent permeability.

At any fibre volume fraction and yarn spacing studied here, the maximum and minimum values for the equivalent permeability of inter-yarn gaps differ by factors of up to 3.3. This may contribute to the wide variation in experimental permeability data for fabrics, and explain why accurate permeability prediction is in practice found to be difficult, even if the fibre volume fraction is known. It illustrates also that, in numerical prediction of textile permeabilities, accurate modelling of yarn cross-sections is critical. If the equivalent permeability of inter-yarn ducts is approximated by the equivalent permeability of ducts with abstracted geometry, the error can be significant even if the duct cross-sectional area is matched.

Approximations for the shape factor and the hydraulic diameter in Poiseuille duct flow were derived as a function the fibre volume fraction, the yarn cross-sectional aspect ratio and the geometrical parameter describing the shape of the power-elliptical yarn cross-section. This allows the equivalent gap permeability to be predicted quantitatively for any fibre volume fraction and yarn cross-section, while more general approximations found in the literature only describe trends for the permeability as a function of the fibre volume fraction.

While geometrically more complex cases may occur in reality, such as gaps bounded by yarns with non-symmetrical cross-section or crimped yarns in woven fabrics, analysis of the simplified case of a uniform single layer of aligned straight yarns allows

fundamental assessment of the sensitivity of fabric permeability to yarn cross-sectional shapes.

Acknowledgement

This work was supported by the Engineering and Physical Sciences Research Council [grant number: EP/IO33513/1], through the EPSRC Centre for Innovative Manufacturing in Composites.

References

[1] Darcy H. Les Fontaines Publiques de la Ville de Dijon. Paris: Victor Dalmont; 1856.
[2] Carman PC. Fluid flow through granular beds. T I Chem Eng-Lond 1937;15:150–6.
[3] Endruweit A, Matthys KS, Peiro J, Long AC. Effect of differential compression on in-plane permeability tensor of heterogeneous multilayer carbon fibre preforms. Plast, Rubber Compos 2009;38(1):1–9.
[4] Gebart BR. Permeability of unidirectional reinforcements for RTM. J Compos Mater 1992;26(8):1100–33.
[5] Lundström TS. The permeability of non-crimp stitched fabrics. Compos Part A-Appl S 2000;31(12):1345–53.
[6] Idelchik IE. Handbook of hydraulic resistance – coefficients of local resistance and of friction. Jerusalem: Israel Program for Scientific Translations; 1966.
[7] Shah RK, London AL. Laminar flow forced convection in ducts. A source book for compact heat exchanger analytical data. New York: Academic Press; 1978.
[8] White FM. Fluid mechanics. 3rd ed. New York (NY): McGraw Hill; 1994.
[9] Ni J, Zhao Y, Lee LJ, Nakamura S. Analysis of two-regional flow in liquid composite molding. Polym Compos 1997;18(2):254–69.
[10] Lundström TS, Frishfelds V, Jakovics A. A statistical approach to permeability of clustered fibre reinforcements. J Compos Mater 2004;38(13):1137–49.
[11] Endruweit A, Long AC. A model for the in-plane permeability of triaxially braided reinforcements. Compos Part A-Appl S 2011;42(2):165–72.
[12] Endruweit A, Zeng X, Long AC. Multi-scale modelling of combined deterministic and stochastic fabric non-uniformity for realistic resin injection simulation. Adv Manuf: Polym Compos Sci 2015;1(1):3–15.
[13] Endruweit A, Ermanni P. Influence of fixation structures on the in-plane permeability of unidirectional glass fiber tapes. J Compos Mater 2002;36(16):1993–2010.
[14] Nedanov PB, Advani SG. Numerical computation of the fiber preform permeability tensor by the homogenization method. Polym Compos 2002;23(5):758–70.
[15] Potluri P, Sagar TV. Compaction modelling of textile preforms for composite structures. Compos Struct 2008;86(1–3):177–85.
[16] Wong CC, Long AC, Sherburn M, Robitaille F, Harrison P, Rudd CD. Comparisons of novel and efficient approaches for permeability prediction based on the fabric architecture. Compos Part A-Appl S 2006;37(6):847–57.
[17] Belhaj M, Deleglise M, Comas-Cardona S, Demouveau H, Binetruy C, Duval C, et al. Dry fiber automated placement of carbon fibrous preforms. Compos Part B-Eng 2013;50:107–11.
[18] Mattsson D, Joffe R, Varna J. Methodology for characterization of internal structure parameters governing performance in NCF composites. Compos Part B-Eng 2007;38(1):44–57.
[19] Olave M, Vanaerschot A, Lomov SV, Vandepitte D. Internal geometry variability of two woven composites and related variability of the stiffness. Polym Compos 2012;33(8):1335–50.
[20] Vanaerschot A, Cox BN, Lomov SV, Vandepitte D. Stochastic framework for quantifying the geometrical variability of laminated textile composites using micro-computed tomography. Compos Part A-Appl S 2013;44:122–31.
[21] Hu J, Liu Y, Shao X. Effect of stitches on the permeability of interbundle channels in stitched fabrics. Text Res J 2003;73(8):691–9.
[22] Nordlund M, Lundström TS. Numerical study of the local permeability of noncrimp fabrics. J Compos Mater 2005;39(10):929–47.
[23] Endruweit A, Long AC. Analysis of compressibility and permeability of selected 3D woven reinforcements. J Compos Mater 2010;44(24):2833–62.
[24] Zeng X, Endruweit A, Brown LP, Long AC. Numerical prediction of in-plane permeability for multilayer woven fabrics with manufacture-induced deformation. Compos Part A-Appl S 2015;77:266–74.
[25] Gunn DJ, Darling CWW. Fluid flow and energy losses in non-circular conduits. Trans Inst Chem Eng 1963;41:163–73.
[26] TexGen (Version 3.5.2). University of Nottingham; 2012. http://texgen.sourceforge.net [viewed 27.09.2012].
[27] Grouve WJB, Akkerman R. An idealised bc for the meso scale analysis of textile impregnation processes. In: The 9th international conference on flow processes in composite materials, Montréal; 2008.
[28] Beavers GS, Joseph DD. Boundary conditions at a naturally permeable wall. J Fluid Mech 1967;30(1):197–207.
[29] Pillai KM. Modeling the unsaturated flow in liquid composite molding processes: a review and some thoughts. J Compos Mater 2004;38(23):2097–118.
[30] Cornish RJ. Flow in a pipe of rectangular cross-section. Proc R Soc Lond A-Conta 1928;120(786):691–700.
[31] Endruweit A, Zeng X, Long AC. Effect of specimen history on structure and in-plane permeability of woven fabrics. J Compos Mater 2015;49(13):1563–78.
[32] Arbter R, Beraud JM, Binetruy C, Bizet L, Bréard J, Comas-Cardona S, et al. Experimental determination of the permeability of textiles: a benchmark exercise. Compos Part A-Appl S 2011;42(9):1157–68.
[33] Mortensen NA, Okkels F, Bruus H. Reexamination of Hagen-Poiseuille flow: shape dependence of the hydraulic resistance in microchannels. Phys Rev E 2005;71:057301.
[34] Bahrami M, Yovanovich MM, Culham JR. Pressure drop of laminar, fully developed flow in microchannels of arbitrary cross-section. ASME J Fluid Eng 2006;128:1036–44.
[35] Gommer F, Brown LP, Wedgewood KCA. Analytical method using gamma functions for determining areas of power elliptical shapes for use in geometrical textile models. Compos Part A-Appl S 2016;81:222–4.
[36] Swery EE, Kelly P, Walbran WA, Bickerton S. Numerical permeability prediction of woven textiles at different compaction levels. In: 11th international conference on textile composites, Leuven; 2013.